THE ASTROPHYSICAL JOURNAL, 405:168–178, 1993 March 1

A NEW X-RAY SPECTRAL OBSERVATION OF NGC 1068

F. E. MARSHALL, H. NETZER,[1] K. A. ARNAUD,[2] E. A. BOLDT, S. S. HOLT, K. M. JAHODA, R. KELLEY,
R. F. MUSHOTZKY, R. PETRE, P. J. SERLEMITSOS, A. P. SMALE,[3] J. H. SWANK,
A. E. SZYMKOWIAK, AND K. A. WEAVER[2]
Laboratory for High Energy Astrophysics, NASA/Goddard Space Flight Center, Greenbelt, MD 20771
Received 1992 May 21; accepted 1992 September 8

ABSTRACT

The first moderate-resolution (FWHM ~ 100 eV) X-ray spectrum of a Seyfert 2 galaxy was obtained with the BBXRT experiment aboard *Astro-1*. The observed X-ray continuum of NGC 1068 from 0.3 to 10 keV is well fitted as the sum of two power-law spectra with no evidence for absorption intrinsic to the source. Strong Fe K emission lines with a total equivalent width of 2700 eV were detected due to iron less ionized than Fe XX and to iron more ionized than Fe XXIII. Unresolved Fe L lines with a total equivalent width of 340 eV were also seen. No evidence was seen for lines due to the recombination of highly ionized oxygen with an upper limit for the O Lyα emission line of 40 eV. The discovery of multiple Fe K and Fe L emission lines clearly indicates a broad range of ionization states for this gas. The X-ray emission from NGC 1068 is thought to be due to radiation from the obscured nucleus of the galaxy that is Compton-scattered by warm ($T \sim 2 \times 10^5$ K) electrons above the obscuring material. We associate the cooler, less ionized Fe with the warm electrons producing the polarized optical light, and the hotter ($T \sim 4 \times 10^6$ K), highly ionized Fe with a previously unseen component. The two components may share the same volume, or the hot component may be located closer to the nucleus. The X-ray emission from the two components is modeled for various geometries using a photoionization code that calculates the temperature and ionization state of the gas. We present models consistent with the X-ray, UV, and optical observations. Typical model parameters are a total Compton depth of a few percent, an inner boundary of the hot component of about 1 pc, and an inner boundary of the warm component of about 20 pc. All the successful models require that oxygen be underabundant compared with solar by a factor of at least 5, while Fe is most likely overabundant. We show that the observed optical and UV line strengths from the NLR are consistent with these abundances.

Subject headings: galaxies: individual (NGC 1068) — galaxies: Seyfert — radiation mechanisms: miscellaneous — X-rays: galaxies

1. INTRODUCTION

Optical spectropolarimetry by Antonucci & Miller (1985) showed that the archetypical Seyfert 2 galaxy NGC 1068 contains a Seyfert 1 nucleus that is obscured from our direct view. A small fraction of the nuclear luminosity is scattered into our line of sight and thereby polarized. The wavelength independence of the polarization in the optical and now in the UV (Code et al. 1991) is compelling evidence that the photons are scattered by electrons. This picture of a hidden nucleus may apply to many Seyfert 2 galaxies. Spectropolarimetry by Miller & Goodrich (1990) found evidence for hidden broad-line regions in four other Seyfert 2 galaxies. There is substantial supporting evidence for this picture. The large equivalent width for the Fe K X-ray emission line predicted by Krolik & Kallman (1987) was found by Koyama et al. (1989) for NGC 1068. The relative weakness in soft X-rays of Seyfert 2 galaxies compared with Seyfert 1 galaxies (Kriss, Canizares, & Ricker 1980) is consistent with an obscured central source. Pogge (1988) found cones of highly ionized gas in the cores of several Seyfert 2 galaxies suggesting that parts of the surrounding galaxy see a more intense ionizing continuum than is seen along our line of sight. Using the ratio of UV lines, Kinney et al. (1991) also argue for an unseen continuum in a number of Seyfert 2 galaxies.

By far the most detailed studies have been of NGC 1068. Miller, Goodrich, & Mathews (1991, hereafter MGM) have mapped the optical polarization in the center of NGC 1068. Comparing the width of the polarized Hβ line seen from the nucleus to that seen from off-nucleus, they conclude that the average temperature of the scattering electrons is ~(2–3) $\times 10^5$. The location, size, and structure of the scattering medium have not been directly measured. Recent *Hubble Space Telescope* (*HST*) observations of the core of NGC 1068 at a continuum wavelength of 5470 Å by Lynds et al. (1991) show an extended cloud with an unresolved peak containing ~20% of the light. Small-aperture spectral observations of this peak by Caganoff et al. (1991) did not detect broad Hβ emission, and the authors concluded that this peak is not the mirror which reflects light from the hidden nucleus. MGM compared predictions of models with various scattering cloud geometries and ionizing continuum shapes with existing optical and X-ray data. They pointed out the difficulty in reconciling the low temperature deduced from the Hβ profiles with the high ionization implied by the lack of low-energy X-ray absorption. However, a small range of models with clouds having an inner radius of about 10^{20} cm and Compton depths of a few percent appeared consistent with the data.

We report in § 2 a new X-ray observation of NGC 1068. The improved spectral resolution ($R \sim 40$) and broad energy range provide important new constraints on models for this galaxy. Section 3 compares these new observations with model predictions. The results are discussed in § 4. Finally, § 5 is a summary

[1] NAS/NRC Research Associate on leave from Tel Aviv University.
[2] Also University of Maryland.
[3] Also Universities Space Research Association.

of the results. We have adopted a distance of 22 Mpc and a redshift of 0.0036 for the nucleus of NGC 1068.

2. OBSERVATION AND DATA ANALYSIS

The Broad Band X-Ray Telescope (BBXRT) was flown as part of the *Astro-1* payload on the Space Shuttle Columbia in 1990 December. BBXRT consists of two nearly identical telescopes (designated A and B) whose conical foil optics focus X-rays onto segmented solid-state detectors. Each detector has five pixels—a small central pixel (designated A0 or B0) and four outer quadrants surrounding the central pixel. The experiment's moderate spectral resolution (ranging from $\sim$90 eV at low energies to $\sim$160 eV at 6 keV), low background, and extended energy range (from $\sim$0.3 to 12 keV) provide important capabilities never before available for the study of Seyfert galaxies. The relatively large effective area (300 cm^2 at 2 keV and 140 cm^2 at 7 keV) means that high-quality spectra can be obtained in a few thousand seconds for sources 1000 times weaker than the Crab Nebula. Serlemitsos et al. (1992) and Weaver (1993) provide a more detailed description of the experiment.

The BBXRT observation of NGC 1068 began at 0^h GMT on 1990 December 9, and 2586 s of data were obtained with the target very nearly centered on the BBXRT detectors. We have chosen data to exclude time intervals contaminated with the soft X-ray emission often seen with BBXRT from the Earth's sunlit atmosphere. The response of the instrument is based primarily on prelaunch measurements of the effective area of the mirrors and the efficiency of the detectors, but some adjustments were made based on our observation of the Crab Nebula. Some additional refinements, such as adjusting the mirror reflectivity at the M-edge of gold, remain to be done. The gain of the detectors has been determined using both an in-flight ^{55}Fe calibration source and lines observed from the Earth's atmosphere. We are confident that the remaining adjustments will at most make minor quantitative changes in the results presented here. Since additional calibration is needed for the B0 pixel at energies less than 3 keV, only data from the A0 pixel will be used in fitting the data at these energies. Data from A0 and B0 pixels have been combined for fitting the higher energy data.

The X-ray spectrum of NGC 1068 is complex, with a hard power-law continuum above $\sim$3 keV and a much softer spectrum at lower energies. There are also strong emission lines in the Fe K band near 6.6 keV and at $\sim$870 eV. The measured continuum spectrum is qualitatively similar to previous observations. Using *EXOSAT*, Elvis & Lawrence (1988) found a two-component spectrum with little evidence for any intrinsic absorption and marginal evidence for a strong Fe K emission line. Using more recent observations with *Ginga* Koyama et al. (1989) found clear evidence for the Fe K line with an equivalent width of 1300 eV and also determined more accurately the spectral index of the hard X-ray power law. The BBXRT data are consistent with a photon index at high energies of 1.5 and the Galactic column density of 3×10^{20} (Lockman 1991), and we have adopted these values. As shown in Figure 1, the sum of two power-law components provides a good fit to the X-ray continuum. The best-fit steep component has a photon index of 3.4 ± 0.4 (unless stated otherwise, all errors correspond to 90% confidence intervals) and a flux of 2.1×10^{-3} photons $cm^{-2}\ s^{-1}\ keV^{-1}$ at 1 keV. The spectral index of the flat component is poorly constrained with the BBXRT data; values between 0.25 and 2.0 are acceptable. We have assumed the best-fit photon index of 1.5 from the *Ginga* observation; the normalization of this component from the BBXRT observation is a flux of 4.8×10^{-4} photons $cm^{-2}\ s^{-1}\ keV^{-1}$ at 1 keV. The continuum luminosity in the 2–10 keV band, assuming isotropic emission at a distance of 22 Mpc, is 2.0×10^{41} ergs s^{-1}. Although the fractional statistical uncertainty in this number is small, the absolute normalization of the BBXRT effective area is probably not known to better than 20%. The luminosity is consistent with the $3 \pm 1 \times 10^{41}$ ergs s^{-1} reported by Koyama et al. The luminosity for the entire 0.3–10 keV band of BBXRT is 9.7×10^{41} ergs s^{-1}; extrapolating this spectrum to 20, 100, or 500 keV increases the X-ray luminosity to 1.1×10^{42}, 1.7×10^{42}, or 3.1×10^{42} ergs s^{-1}.

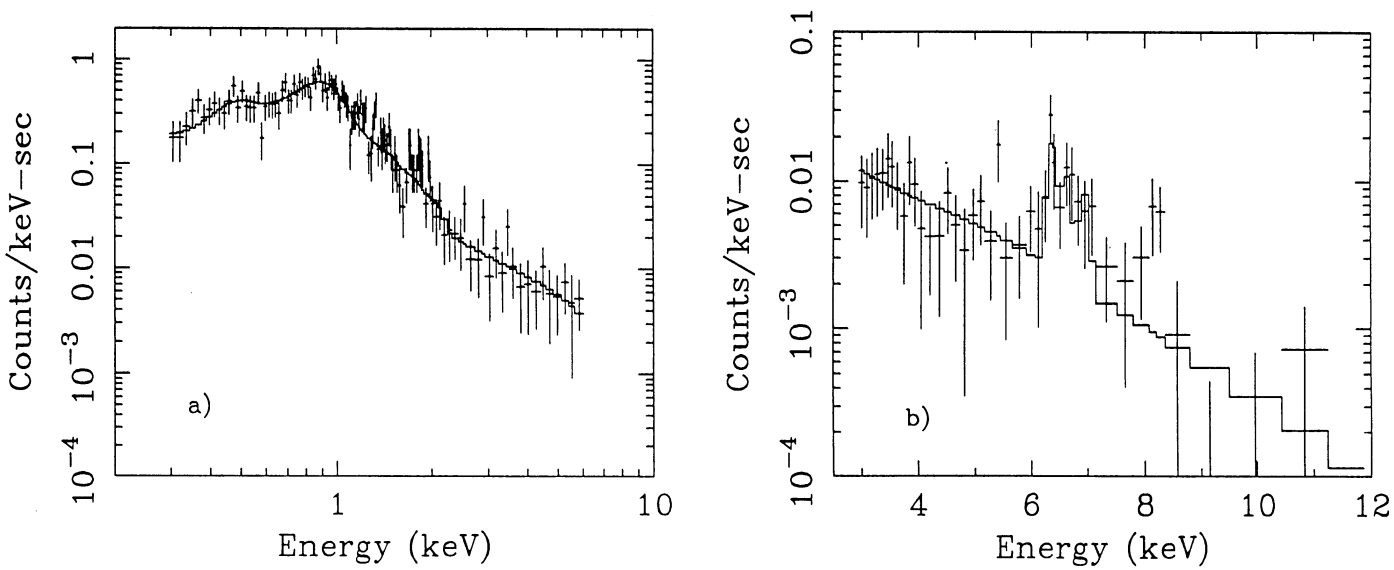

FIG. 1.—Spectrum of NGC 1068 as seen with BBXRT shown separately at (*a*) low energies and (*b*) high energies. The solid line is the best-fit model folded through the BBXRT response function. The spectrum has been corrected for the internal background of the detectors.

There is clear evidence for emission lines in the BBXRT data. In the low-energy data there is a broad excess at about 870 eV which we believe is due to unresolved Fe L lines. For descriptive purposes, we have assumed that the Fe L blend has a Gaussian energy distribution. Best-fit parameters with 90% confidence intervals are a mean energy of 0.87 keV (0.82–0.91 keV), an intrinsic rms width of 0.12 keV (0.09–0.18 keV), and an equivalent width of 0.34 keV (0.24–0.50 keV). Model calculations of NGC 1068 by Band et al. (1990) showed that a wide range of conditions produce strong Fe L-shell emission. However, since the $n = 3$ states of Fe were modeled only schematically in these calculations, quantitative comparisons must be viewed with caution. We note that the observed equivalent width is much smaller than that calculated for optically thin models. The average energy, profile, and intensity of the L-shell emission should provide useful diagnostics for the ionization state and column density of the X-ray mirror when more detailed model calculations are available.

The BBXRT background-subtracted spectrum of NGC 1068 for energies above 3 keV is shown in Figure 1*b*. There is a strong emission feature in the Fe K band centered about 6.5 keV; the feature can be described as either a single broad line or multiple narrow lines. For a single broad line, the best-fit parameters are an equivalent width of 3.8 keV, a line energy of 6.66 keV, and an intrinsic width of 0.40 keV (rms). We are quite confident that our ability to characterize this strong spectral feature is limited almost completely by counting statistics rather than by any uncertainty in the instrument's background or calibration. First, the gain and resolution of the detectors are very accurately known in this energy band because of in-flight calibration using a ^{55}Fe radioactive source which produces lines at 5.9 and 6.5 keV. The detector resolution of 160 eV (FWHM) determined from these lines is in accord with our prelaunch estimates and is easily adequate to resolve a broad line with an intrinsic width of 400 eV (rms). Second, the internal background is much smaller than the measured flux in the Fe K band and contains no obvious spectral features. The ratio of the count rate due to the source to the count rate due to the internal background is about 3 at 5.8 keV, about 8 in the Fe K band, and about 1 at 8.5 keV. The internal background becomes increasingly less important at energies below 5.8 keV. At the highest energies (greater than 8.5 keV), the internal background dominates the total count rate, and the source has not been detected with confidence. The count rate due to the diffuse X-ray background is a very small fraction of the total count rate at all energies. Third, the spectrum of the Crab has been used to calibrate the BBXRT response. As noted above, there are some small adjustments that remain to be made to the BBXRT response, but in this energy band the typical deviation from a smooth continuum has an equivalent width of about 10 eV (comparable to the statistical uncertainty). The comparatively enormous features seen in the spectrum of NGC 1068 cannot be due to problems with the calibration of BBXRT. Finally, relatively few counts were detected from NGC 1068. Each of the points plotted in Figure 1*b* (except the highest energy point) corresponds to between 5 and 9 counts; the error bars indicate the statistical uncertainties.

For a variety of reasons, we have chosen to concentrate our analysis of the Fe K spectral feature on the results of one specific model, although other models can also provide an equally good fit to the data. A model with one broad line has not been chosen because of the difficulty in understanding how such an intrinsically broad line could have such a large equivalent width. For example, a broad line produced in the accretion disk is expected to produce an equivalent width of only a few hundred electron volts, and the equivalent width should not be changed by the scattering needed to reach the observer. Consequently, we chose to interpret the observations in terms of intrinsically narrow lines. Fe Kα lines range from 6.40 keV (in the rest frame) for fluorescence of neutral material 6.97 keV for H-like recombination. If a model with two narrow lines including one due to the fluorescence of neutral material is assumed, the BBXRT data require the other line to have a rest-frame energy of at least 6.65 keV. This requires the existence of very highly ionized Fe and makes the detection of H-like recombinations plausible. The flux in the lines due to neutral material and He-like and H-like recombination can be independently determined because the lines are resolvable with BBXRT's resolution. We have chosen to interpret the BBXRT observation using a model with these three narrow lines; the model produces as good a fit as the model with a single broad line. The best-fit energy of the line due to cool material is 6.36 ± 0.05 keV (or 6.38 ± 0.05 keV in the rest frame). These energies are consistent with the flourescence of material with an ionization state ranging from neutral through Ne-like. We will assume an energy corresponding to neutral material. Additional lines due to other ionization states are also plausible, but we have limited the number of lines to three because of the instrument resolution and the relatively small number of detected photons. Since the He-like triplet cannot be resolved with BBXRT, we will assume a single line at an average rest-frame energy of 6.65 keV.

The best-fit parameters for the model with three narrow Fe lines (fluorescence of neutral material, He-like recombination, and H-like recombination) are as follows. The fluorescence line has an equivalent width of 1.18 ± 0.68 keV (a line flux of 3.94×10^{-5} photons cm^{-2} s^{-1}), the He-like line has an equivalent width of 0.78 ± 0.68 keV (a line flux of 2.43×10^{-5} photons cm^{-2} s^{-1}), and the Lyα line has an equivalent width of 0.74 ± 0.63 keV (a line flux of 2.14×10^{-5} photons cm^{-2} s^{-1}). The addition of these lines reduces χ^2 by 17.5. Removing both the recombination lines increases χ^2 by 6.8, while removing only the Lyα line increases χ^2 by 3.5. We estimate that between 30% and 75% of the Fe K line flux is due to the He-like and H-like recombination lines. The sum of the equivalent widths is 2.70 keV. Assuming that the relative intensities of the lines remain constant, the 90% confidence interval for the total equivalent width covers 1.67–3.73 keV. The equivalent widths are based on an assumed photon index of 1.5. Increasing (decreasing) the index by 0.2 would decrease (increase) the equivalent width of the 6.4 keV line by about 10%, which is considerably less than the statistical uncertainties.

We note that the sum of these equivalent widths is about twice the equivalent width found by Koyama et al. (1989). As discussed below, the scattering region in NGC 1068 is expected to be so extended that a large variation during an interval of several years should not be seen. Although the statistical uncertainty in the *Ginga* measurement is only 0.1 keV, Koyama et al. estimate that fluctuations in the X-ray background increase the range of the 90% confidence interval to 0.8–2.0 keV. Since the 90% confidence intervals overlap by a substantial amount, there appears to be no real conflict between the results. Since the sum of the BBXRT line fluxes is only 25% larger than the *Ginga* line flux, the data are consistent with the idea that continuum flux from NGC 1068 was overestimated in the *Ginga* observation owing to fluctuations.

We have simulated the *Ginga* response to the best-fit BBXRT model and verified that fitting a single narrow line produces nearly the same equivalent width as the total of the individual equivalent widths of the three lines of the model. We also verified that the best-fit line energy is consistent with that observed with *Ginga*. Koyama et al. argue that fluctuations should not have a large effect on the spectral index measured with *Ginga*.

The lack of spectral features due to O also provides important constraints for models of NGC 1068. For neutral material of solar abundances, oxygen provides much of the X-ray opacity in the BBXRT energy band. The lack of absorption intrinsic to NGC 1068 indicates that the scattering medium must be highly ionized (Monier & Halpern 1987). As discussed below, recombination onto highly ionized oxygen can produce a strong emission-line feature. The 90% confidence upper limit to O Lyα is 4.0×10^{-4} photons cm^{-2} s^{-1}, or an equivalent width of 40 eV; the limit for He-like recombination lines is comparable. The O absorption edge ranges from 530 to 870 eV depending on the ionization state. The presence of the Fe L emission feature complicates the search for an absorption edge, since the exact structure of the emission lines is not known. We believe that an optical depth of unity is a conservative upper limit for an edge at 870 eV. Smaller limits can be set at lower energy edges, if one makes the reasonable assumption that the Fe L line center does not move below 870 eV.

NGC 1068 contains many starburst knots (Bruhweiler, Truong, & Altner 1991) within the BBXRT field of view. Although the typical X-ray spectrum of a starburst nucleus is not known, young supernova remnants (SNRs) may make a substantial contribution. Young SNRs in our Galaxy often show intense X-ray line emission from the He-like triplets of Si and S (Holt 1983), but there is no compelling evidence for these lines in the spectrum of NGC 1068. There is marginal evidence ($\Delta\chi^2$ of 2.7) for the Si triplet with an equivalent width of 84 eV at 1.86 keV, but some of this emission is due to the fluorescence of Si in the detector itself. A conservative upper limit for the equivalent width of the Si triplet is about 170 eV. There is no indication of the He-like S lines; the upper limit for the equivalent width is 165 eV. These limits are much smaller than the equivalent widths found for Cas A or Tycho remnants, indicating that either the starburst knots make a small contribution to the X-ray flux at these energies or that their X-ray spectrum is not similar to these young remnants.

Including in the fit a narrow line at 8.27 ± 0.14 keV with a line flux of 4×10^{-5} photons cm^{-2} s^{-1} (an equivalent width of 1.57 keV) reduces χ^2 by 5.8. As is the case with the Fe lines, we are confident that the uncertainty in the determination of the line flux is dominated by counting statistics rather than uncertainties in our knowledge of the calibration or instrument background. Although the probability of a reduction this large due to chance alone is less than 2% for any particular energy, there are numerous possible energies. Thus we are not that unlikely to find a line reducing χ^2 by this amount somewhere in the spectrum. In addition, the reduced χ^2 of 0.7 without this line indicates a good fit. We conclude that the evidence is not sufficient to claim detection of this line with certainty. We note that the energy of this line is consistent with that of Ni Lyα, but there are many difficulties with such an interpretation. The redshifted energy of this Ni line (8.06 keV) is outside the 90% confidence interval, and if we assume this energy, the reduction in χ^2 for the addition of this line, whose equivalent width is 0.60 keV, is only 1.4. Second, assuming that Ni and Fe Lyα emission come from the same region, the ratio of fully ionized Ni to Fe is about 0.5, or about 10 times the relative solar abundances of Ni and Fe. Finally, there are no indications of lines due to less ionized Ni such as were seen for Fe.

3. MODEL CALCULATIONS

3.1. *General Considerations*

Our model for the nucleus of NGC 1068 follows the first paper by Antonucci & Miller (1985) and the detailed work of MGM. We also assume a cylindrical geometry with a "normal" Seyfert 1 nucleus at its center. A central, molecular torus with a thickness of about 1 pc obscures the continuum source and the broad-line region (BLR) from our direct view. This continuum and the broad emission lines are seen through reflection by dust and by warm electrons. Scattering by dust, which takes place far from the center, was used by MGM to deduce the intrinsic broad-line widths. This region is not discussed in our paper. The electron scattering region is located about 1″ from the hidden BLR (Lynds et al. 1991; Caganoff et al. 1991) at about the innermost radius of the narrow-line region (NLR). Scattering in this region is probably due to warm electrons, since the reflected broad emission lines are broader than the intrinsic lines (assuming that the dust scattering does not alter the line shapes), and the polarization percentage is angle-independent. Comparing the "intrinsic" and reflected line widths, MGM estimated an electron temperature of about (2–3) $\times 10^5$ K in this region. The scattered continuum radiation is about 16% polarized, indicating a mean scattering angle of 32°.

This relatively small scattering angle means that we are viewing the torus close to face-on, and it is easy to envision geometries in which a sizable fraction of the inner face of the torus would be directly visible. Reflection of X-rays from this optically thick material would produce a "hard" spectrum with intense Fe K line emission (e.g., Lightman & White 1988). Such a component would contribute to the Fe K line flux seen from NGC 1068, but there is no evidence for a reflection component in the spectrum of NGC 1068 in either the BBXRT of the *Ginga* data. Consequently, we have assumed that none of the torus is directly visible. It is possible that our view of the central source and the torus is blocked by an obscuring cloud rather than by the torus itself.

MGM assumed that the heating and ionization of the reflecting material are due to the central optical-UV continuum and that the gas density had a r^{-2} radial profile. Although accurate X-ray absorption measurements were not available, it was known that the optical depth due to photoelectric absorption at 1 keV could not be much larger than unity. MGM found it "difficult, but not impossible," to construct models with temperatures as low as 3×10^5 K as required by the optical spectrum and at the same time avoid substantial absorption at 1 keV by ionizing the metals and reducing the Compton depth. For reasonable values of the intrinsic luminosity, this required the inner face of the reflecting cloud to be at least 10^{20} cm from the nucleus. The most successful models (i.e., those satisfying the contraints on the gas temperature, X-ray absorption, and intrinsic luminosity) had boost factors, the ratio of the observed to the unobscured flux, from 10^2 to $10^{2.6}$ and Compton depths of a few percent.

Our basic model stems directly from the more successful MGM models (see their Table 1, models 61.2Q and 61.3Q), but changes are now needed because of the new X-ray absorption,

O recombination line, and Fe K line observations of BBXRT. As explained below, we require an additional hot ($\sim 4 \times 10^6$ K) component and changes in the chemical abundances. We also treat in some detail the material in the NLR, since this is relevant to our discussion of the chemical composition of the gas. Thus our basic model includes three directly visible components which are referred to as the "cold" (NLR, $\sim 1 \times 10^4$ K), "warm" ($\sim 2 \times 10^5$ K), and "hot" ($\sim 4 \times 10^6$ K) components.

We have assumed that the X-ray spectrum is produced entirely by the illumination of visible material by X-rays emitted in the obscured nucleus. Since the entire galaxy is in the BBXRT field of view, discrete nonnuclear X-ray sources will also contribute to the spectrum. The high luminosity, the shape of the continuum, and the large Fe equivalent width all indicate that contributions of discrete sources must be small. Recent results from the observation (Halpern 1992; Wilson et al. 1992) with the *ROSAT* high-resolution imager (HRI), which has a spatial resolution of a few arcseconds, shows that most of the observed soft ($E < 2$ keV) flux is unresolved. Wilson et al. report 55% of the flux due to the point source, 23% due to emission extended by a few arcseconds, and 22% of the flux due to emission extended by about 90″. They also show the most extended component to have a harder spectrum and suggests that this component may be the dominant contributor to the higher energy (>2 keV) flux seen by other observers. We note that the hard power-law component measured with BBXRT will contribute only about 3% of the observed HRI count rate and consider it unlikely that such a small contributor would dominate the spectral differences observed with the HRI. The observed power-law spectrum and intense Fe K line emission also strongly argue that the hard component seen with BBXRT is not the extended component seen with the HRI. The equivalent width of the Fe K lines, for example, is much larger than that seen from X-ray binaries, and there are no strong lines of Si or S such as have been seen in many SNRs in our Galaxy. As discussed in § 4, we believe the existence of these spatially extended components has limited impact on our results.

3.2. *Components of the Model*

The four components of our model are the obscured Seyfert 1 (a nonstellar continuum source and a BLR) nucleus with the obscuring torus and the three directly visible components mentioned earlier. We fix the opening half-angle of the torus at 35°, but somewhat different angles are also acceptable. For the "warm" and "hot" components we assume a one-sided geometry with all reflection and line emission taking place only on the side closer to the observer. We assume a symmetric two-sided geometry for the "cold" (NLR) component. A schematic representation of this geometry is shown in Figure 2.

The optical-UV continuum radiation from the nucleus is taken to be that of an accretion disk (e.g., Laor & Netzer 1989) with a simple limb-darkening pattern:

$$I(\theta) = I_0 \cos\theta(1 + 2\cos\theta),$$

where θ is the angle to the symmetry axis of the system. For simplicity the same pattern is used for the X-ray emission, although it probably does not arise in the disk (Laor 1990). Assuming isotropic X-ray emission would change the ratio of the 10 eV and the 1 keV fluxes by a factor of 2, but would not change the total luminosity substantially. We assume that the torus reprocesses the continuum that it intercepts and radiates

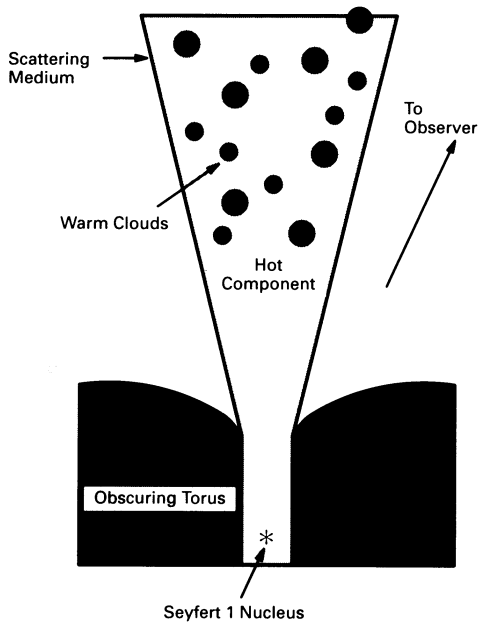

FIG. 2.—Schematic diagram of our model for NGC 1068

isotropically in the infrared. The normalization of the continuum is then determined by the observed luminosity of the nuclear infrared source of 8.6×10^{44} ergs s^{-1} (Telesco et al. 1984). Given the opening angle, the disk radiation pattern, and an average illumination angle of the cone material of about 30°, the integrated luminosity at energies greater than 1 ryd is 2×10^{45} ergs s^{-1}, and the luminosity at energies greater than 1 keV is 1×10^{44} ergs s^{-1}. This makes NGC 1068 about as luminous as NGC 5548 at optical and X-ray energies—somewhat surprising in view of its low redshift. With this choice the continuum "boost factor" is about 300. Finally, we assume the intrinsic FWHM of Hβ to be 2900 km s^{-1} (see MGM) and the intrinsic (unobscured) equivalent width of the broad Hβ line ($W_{H\beta}$) to be in the range 100–200 Å. This point is essential to the rest of the analysis and is discussed below.

The optical spectrum of the "cold" NLR is well known and has been discussed in several earlier publications (e.g., Shields & Oke 1975; Koski 1978; Neugebauer et al. 1980; Ferland & Osterbrock 1986). As argued by MGM, scattering by this component is only a small fraction of the observed continuum. Consequently, they did not calculate a specific NLR model. Our detailed modeling confirms this conclusion as shown below.

The "warm" ($T \sim 2 \times 10^5$) component reflects the observed continuum and the broad Hβ line and produces most of the Kα iron line at 6.4 keV. This is the only component discussed by MGM, and our initial guess about its location and density follows from their modeling. We chose the simplest possible geometry for this component: a scattering angle of 32° as implied by the percentage polarization of 16%, a mean illumination angle of 30°, and uniform distribution of material inside the cone. Our BBXRT observations provide several new constraints on the warm component: the upper limit (40 eV) on the equivalent width of O VIII λ19, the measured strength of the broad 870 eV feature attributed to iron L line emission, and the upper limit on the continuum absorption in the range 0.3–10 keV. All of these were unknown to MGM and necessitate a modification of their model.

The "hot" ($T \sim 4 \times 10^6$) component emits the observed lines of Fe XXIV, Fe XXV, and Fe XXVI at 6.7–6.9 keV. This component was not considered by MGM, who had no spectral information on the Kα lines and thus assumed that the entire feature is from the warm gas. MGM observed the broad Hβ line, in reflection, in several condensations and concluded that the off-nucleus polarization is due to dust reflection. According to them, the good agreement between the electron-scattered and the dust-scattered $W_{H\beta}$ of about 120 Å is strong evidence against a very hot component. If such a hot component existed, the nuclear $W_{H\beta}$ would be smaller than the dust-scattered $W_{H\beta}$ because scattering by the hot gas would broaden the Hβ profile beyond recognition (MGM, Fig. 9) but will not affect the continuum. We note, however, that the uncertainty on the optical continuum polarization is about 25%. We further note that some of the continuum radiation reflected by dust, in the northeast knot, may be starlight and not the central nonstellar continuum. The combination of the two amounts to an uncertainty of a factor of about 2 in the intrinsic $W_{H\beta}$ (J. Miller 1992, private communication). Thus, the hot component contribution to the observed scattered continuum is at most 50%. As we show later, this is similar to the amount needed to explain the 6.7–6.9 keV lines.

We allow for the hot and warm components to occupy the same volume, but this is not required in all of our solutions (see below). The fraction of the continuum radiation reflected by each component in the observer's direction is (MGM)

$$f_{\rm scat} = 1.29\tau_{\rm es} c_f \Omega/4\pi ,$$

where Ω is the solid angle, c_f is the covering fraction, $\tau_{\rm es}$ is the Compton depth, and 1.29 is the scattering anisotropy factor appropriate for the assumed 32° angle. We have assumed a geometry in which clouds exist within a solid angle Ω, but there are lines of sight that do not intercept any cloud. All the clouds have the same inner and outer boundaries. The Compton depth is for a line of sight through one of the clouds. We also define a filling factor f_f as the fraction of the volume within the clouds that has material. For the models considered here the sum of $f_{\rm scat}$ over all components is 0.0035, corresponding to a boost factor of 286.

We also define y_w (y_h) as the fraction of the total scattered flux due to the warm (hot) component. As is shown later, the calculated contribution of the cold component (y_c) is very small. The $W_{H\beta}$ observed in polarized light is reduced relative to the intrinsic $W_{H\beta}$ by y_w.

3.3. *Photoionization Calculations*

We used the code ION, most recently described in Rees, Netzer, & Ferland (1989), to calculate the ionization and thermal structure for the cool, warm, and hot components in the nucleus of NGC 1068. ION employs a full equilibrium solution for a photoionized gas and takes into account all the important ionization and heating processes. Special care was taken in calculating the inner-shell ionizations and the different Auger transitions, including the ejection of up to 3 secondary electrons. We have included at least two ground-state transitions for each ion which is important in controlling the electron temperature. The continuum assumed for the present calculations is listed in Table 1. We have taken the approach of MGM and approximated unobserved parts by simple power laws. For the unobserved extreme ultraviolet (EUV) part we have extrapolated the BBXRT continuum to lower energies, and connected the 10 ryd flux thus obtained to the observed 0.73 ryd flux. The resulting power-law slope (1.07) is similar to the one used by MGM. For extrapolation of the BBXRT flux to high energies, we extrapolated the observed *Ginga* power law of slope 0.5 in energy up to an abrupt cutoff at 100 keV. We have experimented with several variants of this continuum, such as increasing the unobserved ultraviolet flux and decreasing the hard X-ray cutoff energy to 50 keV. None of these made a large change to the results, and we restrict our discussion to this one choice. The photoionization models for the three components are defined by the ionization parameter U (the ratio of the incident flux of ionizing photons to the H number density) calculated at the illuminated face of the cloud, the gas density, and the chemical composition.

TABLE 1

ADOPTED CONTINUUM

Energy (ryd)	Energy (eV)	log Flux (ergs s^{-1} cm^{-2} Hz^{-1})
1×10^{-5}	1.36×10^{-4}	−30.0
1×10^{-4}	1.36×10^{-3}	−23.6
1×10^{-3}	1.36×10^{-2}	−23.16
0.2	2.72	−25.458
0.73	9.93	−25.5
10	136	−26.72
22.06	300	−27.55
73.5	1×10^3	−28.765
220.6	3×10^3	−29.55
735	1×10^4	−29.98
3670	5×10^4	−30.33
7350	1×10^5	−30.48

For the cold component we only calculate the intensity of some strong lines. The main observational constraint is the observed flux in the narrow Hβ line (e.g., Neugebauer et al. 1980) with the assumed reddening which we take to be $E(B-V) = 0.4$. This fixes the covering factor for the NLR gas, assuming a radiation-bound dust-free cloud. Note, again, that for this component the assumption is that 50% of the observed flux comes from the opposite side of the nucleus.

The observational constraints on the warm component enable the determination of the ionization parameter and the composition using the Fe and O VIII line intensities. The equivalent width of the iron 6.4 keV line due to fluorescence of the warm component is

$$W_{6.4} \approx 670 y_w (X_{\rm Fe}/4 \times 10^{-5}) \text{ eV} ,$$

where $X_{\rm Fe}$ is the iron abundance relative to hydrogen and we have integrated over the observed continuum above 7.6 keV. After reducing the observed equivalent width of the line (1180 eV) by the 110 eV typically seen for Seyfert 1 galaxies and associated with accretion disk processes (Pounds et al. 1990), we find that the most likely iron abundance in the warm component ranges from 1.5 times solar if the hot component produces a small fraction of the scattered luminosity up to 3 times solar if the hot and warm components produce equal amounts of scattered luminosity. (No corrections have been made for possible contributions to the equivalent width due to resonant scattering [Band et al. 1990]. In our successful models, Fe ions in the warm component either have a full L shell or a nearly full L shell. This substantially reduces the contribution of resonant scattering.) The oxygen in the warm component must be essentially completely ionized to avoid absorption of soft X-rays, and the intensity of the O VIII 19 Å recombination line is proportional to the oxygen abundance.

The relative intensity of the 6.4 keV iron line and the O VIII 19 Å line is proportional to the ionization parameter, the abundance of the elements, and the temperature:

$$\frac{I(\text{Fe 6.4 keV})}{I(\text{O VIII 19 Å})} \approx 1.4\left(\frac{U}{50}\right)\left(\frac{T_e}{2\times 10^5}\right)^{0.8}\left(\frac{X_{\text{Fe}}}{X_{\text{O}}}\right).$$

Contributions to the O VIII 19 Å line due to recombinations in the hot component are very small because of the high temperature. A slight complication in this ratio is the possible destruction of the O VIII line photons due to continuous opacity because of the large number of resonant scatterings. This process is explicitly calculated in ION using the method described in Netzer (1990). We find this process to be important only in those cases where the continuum optical depth at 1 keV is larger than about 0.5. This exceeds, by far, the calculated 1 keV opacity of our best model.

The relative strengths of the Fe L lines and the 6.4 keV lines depend on the temperature and the degree of ionization of iron. Small ionization parameter models give less L emission, since much of the iron is in ions with more than 10 electrons. L-line recombination is important when iron is at least 16 times ionized and the number of lines involved is very large. The only calculations we are aware of for the L-line emission are by Band et al. (1990). The atomic data used by these authors is not available to us. Also, we did not attempt to reproduce the increase in the L-line intensity due to continuum absorption, which is very important for low optical depth lines (Band et al.). Our calculated L-line emission assumes, simply, that one-third of all recombination of the appropriate ions leads to the formation of L emission lines around 870 eV. This simplified approach is associated with a large, unknown uncertainty.

The observation of H-like and He-like recombination lines with comparable intensities requires an ionization parameter large enough so that the most abundant Fe ions are Fe^{+23} to Fe^{+26} (i.e., Li-like to fully ionized). Such a large ionization parameter is associated with high temperatures, as shown below. While $W_{6.4}$ depends primarily on the Fe abundance and the scattered fraction of the warm component, the equivalent widths of the Fe lines due to the hot component depend primarily on the Fe abundance, the scattered fraction of the hot component, the effective recombination coefficients (and thus temperature), and the emission measure of the hot component. We have assumed that the chemical abundances of the warm and hot components are the same, and once a geometry and radial dependence for densities are assumed the ratio of emission measure and scattered fraction is set. With these assumptions and detailed calculations of the effective recombination coefficient, the relative strengths of the Fe lines reveal the relative scattering fraction of the hot and warm components and the ionization parameter for the hot component. The models presented below all have values for the ratio of $I(6.7 \pm 6.9$ keV) to $I(6.4$ keV) consistent with the BBXRT observation, and we assume little contribution to the 6.4 keV line from the cold component. The hot component also produces a thermal X-ray continuum, but we have verified that this is well below the intensity of the reflected continuum at all energies.

Adiabatic cooling of the scattering medium could, in principle, play an important role in determining its temperature. As pointed out by MGM, the observed widths of the polarized optical lines constrain the range of acceptable expansion velocities. We have verified for all our models that the maximum acceptable adiabatic cooling for a uniformly expanding medium with the maximum velocity corresponding to the observed FWHM of the broad lines is a small fraction of the total cooling. Consequently, we have assumed for our models that expansion is not important. Since the relative importance of expansion cooling is an increasing function of radius, this assumption must be violated at sufficiently large distances, but the contribution to the Compton depth at these radii is very small. We have considered models in which the X-ray lines due to highly ionized Fe are produced by the same 2×10^5 K gas that is producing the polarized optical lines. Fluorescence of other cool material would produce in this case the observed line at 6.4 keV. Limiting the expansion velocity again to the maximum velocity corresponding to the observed FWHM of the broad optical lines requires the gas to be at large radii (more than about 40 pc) and a luminosity at least 10 times larger than assumed. Such a large luminosity does not seem plausible, and we do not consider such models further.

The two sets of chemical compositions used for our models are listed in Table 2. Except for O and Fe, the abundances are close to the solar abundances of Anders & Grevesse (1989). In both cases we have used the most likely Fe abundance as deduced from the observed $W_{6.4}$ and (nearly) the largest oxygen abundance consistent with the lack of a detectable O VIII 19 Å line. The first set, referred to as the "high-Fe model," is used for models in which half of the continuum reflection is due to the hot component. The resulting iron abundance is about 3 times the adopted solar value of 4.0×10^{-5}, and the oxygen abundance is about one-fifth of the adopted solar value of 8.5×10^{-4}. There are no strong constraints on the remaining abundances from the hot and the warm components, but the observed NLR spectrum suggests that their composition is nearly solar. Our second choice of abundances, referred to as the "moderate Fe model." is required for fitting the observed spectrum in a case where most of the reflection is due to the warm component.

Because of the evidence for gas with two very different temperatures, we seek a solution whereby hot ($\sim 4 \times 10^6$ K) and warm ($\sim 2 \times 10^5$ K) components coexist in the nucleus, possibly in pressure equilibrium. The calculated T_e versus U/T_e relation for gas with the "high-Fe" composition is shown in Figure 3. The diagram is equivalent to the T versus $P_{\text{rad}}/P_{\text{gas}}$ (or T versus Ξ) relationship, which has been studied, in greater detail, in relation to the confinement of the BLR clouds (see Krolik, McKee, & Tarter 1981; Kallman & Muchotzky 1985). While this two-phase picture was considered an appealing idea for some time, it was recently shown (Mathews & Ferland

TABLE 2

ASSUMED ABUNDANCES

ELEMENT	ABUNDANCES RELATIVE TO H	
	High-Fe Model	Moderate-Fe Model
H	1.0	1.0
He	0.1	0.1
C	3.0×10^{-4}	3.0×10^{-4}
N	1.0×10^{-4}	1.0×10^{-4}
O	1.5×10^{-4}	1.0×10^{-4}
Ne	1.0×10^{-4}	1.0×10^{-4}
Mg	3.3×10^{-5}	3.3×10^{-5}
Si	3.3×10^{-5}	3.3×10^{-5}
S	1.6×10^{-5}	1.6×10^{-5}
Fe	1.2×10^{-4}	0.6×10^{-4}

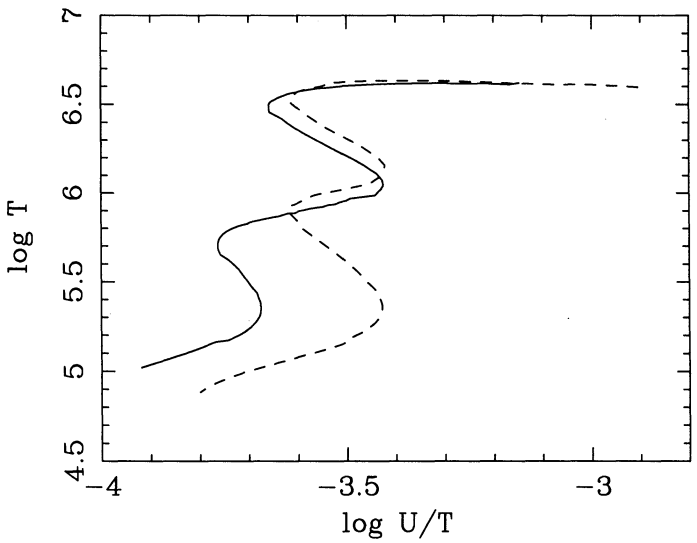

FIG. 3.—The log T vs. log (U/T) relation for the assumed NGC 1068 continuum at the inner face of the warm clouds (*solid line*) and at a Compton depth of 0.025 (*dashed line*) for the "high-Fe model" composition.

1987) to have some problems because of the too low Compton temperature predicted for the confining gas.

The hot gas in our model of NGC 1068 is not related to the BLR. Its Compton temperature is very low, about 4×10^6 K, because of the extremely strong soft X-ray continuum which provides much Compton cooling. The calculated temperature depends on location because there is some buildup of opacity, especially in the warm gas; regions exposed to the direct radiation from the central source have lower temperatures compared with those behind warm gas clouds. The two curves shown in Figure 3 demonstrate this effect. The curve shown with the solid line is relevant to the inner face of the warm cloud and is not affected by opacity. There is a clear change of slope and several stable solutions, but they do not overlap. The second curve (*dashes*) is applicable at a location where the Compton depth in the warm gas is about 0.025 and the shape of the continuum has been modified by attenuation. In this location there is a clear, narrow region of instability with a two-phase solution. The warm and the hot components in NGC 1068 can thus coexist in some parts of the nucleus. NGC 1068 is the only Seyfert galaxy where the two components are actually observed, making the two-phase solution more than a purely theoretical concept. Our following discussion is based on that, and we search for a pressure equilibrium solution for the hot and the warm components. In particular, we consider the case where the two temperatures differ by a factor of 20.

Two profiles were used for the radial dependence of the gas density; in each case, we assume the same profile for the gas in the warm and hot components. In the first profile, the density scales as r^{-2}, as appropriate for a constant-velocity model. This profile produces a uniform ionization parameter throughout the volume. In the other profile, the density scales as $r^{-1.5}$, as appropriate for free fall or decelerated outflow. This profile produces $U \propto r^{-0.5}$. These assumptions are not meant to represent a full dynamical solution of the gas flow in the nucleus of NGC 1068. They are simply natural choices to describe such a flow. We do not require the flow to originate (or terminate) at the center, and allow for the possibility of injecting material at a given location. As already discussed, we assume steady state solutions for the temperature and no instabilities.

The parameters of our three generic models are listed in Table 3. Acceptable values for the ionization parameter U of the warm component are strongly constrained by the lack of X-ray absorption and the average temperature determined from the optical data. The values depend somewhat on the chemical abundances (Fe overabundance provides additional cooling, for example) and atomic data,[4] but we estimate that U cannot cover more than a range of about 2 in successful models. For all our models we have used a value of U of 49.3 at r_{in}. Once y_w has been chosen, there is little choice for r_{in} of the warm component (see scaling relationships below). For convenience we have chosen the same r_{in} (and thus density) for models 1, 2, and 3. The warm-component temperature ranges from 1.75×10^5 to 2.3×10^5 K—values consistent with that derived from the optical polarization data. The density of the hot component is chosen to produce approximately the same pressure for the warm and hot components, which requires a ratio of about 20 in temperature and density. Ionization states of Fe that have at least 10% of ions are indicated for both components. The calculated line and continuum intensities for the models are given in Table 4. Each of the models produces O Lyα, Fe L, Fe Kα, and Fe recombination fluxes consistent with the observations.

The observed optical-ultraviolet emission-line spectrum provides another crucial test for the low O-to-Fe ratio deduced from the X-ray measurements. The line emission in the optical and UV bands has been calculated for a typical NLR cloud exposed to the same nuclear luminosity as the warm and hot components. The model parameters for this cold component are given in Table 5; the calculated line fluxes are compared to observed fluxes (Snijders, Netzer, & Boksenberg 1986; Kriss et al. 1992) in Table 6. There is clear evidence for reddening of the narrow emission lines in this source (Snijders et al. 1986 and references therein), and we have adopted a simple $1/\lambda$ extinction law with $E(B-V) = 0.4$ mag. Our intention is to show the result for a "typical" narrow-line cloud, which is a highly simplified picture of the real situation where a range of densities and ionization parameters must be present. This choice gives, however, a reasonable agreement with the observed intensity of most strong lines. In particular, the strong [O III] 5007 and 4959 Å lines are only slightly weaker than observed, despite the very low oxygen abundance. The most noticeable difference from the spectra of other active galactic nuclei (AGNs) is the extremely weak O III] 1664 Å line, which we attribute to the low oxygen abundance. Note that the observed ratio of He II λ4686 to Hβ suggests that we have underestimated the UV continuum around 4 ryd.

3.4. *Scaling Relationships*

We have presented only three models, but the following approximate scaling relationships can be used to estimate other acceptable combinations of parameters and to explore the effects of different assumptions. The relationships assume that the ratio of r_{in} to r_{out} remains unchanged, but in general

[4] Soon after the calculations had been completed, we received a preprint by Arnaud & Raymond (1992) with new recombination coefficients for iron. The implementation of these rates in ION caused a change in the best value of the ionization parameter required to obtain the gas temperature of 2×10^5 K. The new value is 39 rather than the 49.3 used here. The change is caused by a small difference in the relative abundance of Fe XV and Fe XVI, which provide the dominant cooling lines for this model. An increase in density by this factor will basically reproduce the same model without affecting the assumed luminosity. We estimate that the above factor of 30% is roughly the uncertainty due to inaccuracies in atomic data.

TABLE 3

MODEL PARAMETERS

Parameter	Model 1	Model 2	Model 3	Model 4
General				
s (in $n \propto r^{-s}$)	1.5	1.5	2.0	2.0
L_{hot}/L_{warm}	0.81	0.31	1.09	1.0
Composition	High Fe	Moderate Fe	High Fe	High Fe
Warm Component				
y	0.55	0.76	0.48	0.5
r_{in} (pc)	20	20	20	2.0
r_{out} (pc)	61	113	154	11
$n(r_{in})$ (cm^{-3})	700	700	700	70000
$U(r_{in})$	49.3	49.3	49.3	49.3
T_{in} (K)	2.4×10^5	2.4×10^5	2.4×10^5	2.8×10^5
T_{out} (K)	1.3×10^5	1.2×10^5	1.7×10^5	2.0×10^5
Fe^{+n}	14–17	14–18	15–17	16–18
τ_{es}	0.03	0.04	0.03	0.014
c_f	0.5	0.68	0.5	...
f_f	...	...	...	0.05
Hot Component				
y	0.45	0.24	0.52	0.5
r_{in} (pc)	1.0	1.0	2.0	2.0
r_{out} (pc)	61	113	154	11.0
$n(r_{in})$ (cm^{-3})	3130	3130	3500	3500
$U(r_{in})$	4410	4410	986	986
T_{in} (K)	4.0×10^6	4.0×10^6	4.0×10^6	3.9×10^6
T_{out} (K)	1.5×10^6	2.5×10^6	3.5×10^6	3.7×10^6
Fe^{+n}	23–26	23–26	24–26	23–26
τ_{es}	0.013	0.01	0.017	0.014
c_f ($r < 20$ pc)	1.0	1.0	1.0	...
c_f ($r > 20$ pc)	0.5	0.32	0.5	...
f_f ($r < 20$ pc)	...	...	...	0.95
f_f ($r > 20$ pc)	...	...	...	0.95

this restriction can be relaxed as long as the ratio is $\ll 1$. All the variables refer to a particular component (e.g., the warm component) except F_{obs}, the observed continuum flux, and L, the intrinsic luminosity:

$$\tau_{es} \propto yL^{-1}c_f^{-1}\Omega^{-1}F_{obs}^{-1} .$$

The inner radius scales as

$$r_{in} \propto yF_{obs}f_f U_{in}^{-1}c_f^{-1}\Omega^{-1}\tau_{es}^{-2} ,$$

where U_{in} is the ionization parameter at r_{in}. The density at a fixed radius (e.g., one pc) scales as

$$n_1 \propto U_{in}^{-1}c_f^{-1}\Omega^{-1}\tau_{es}^{-1} \quad \text{for } \alpha = 2 ,$$

or

$$n_1 \propto U_{in}^{-1/2}c_f^{-1/2}\Omega^{-1/2}f_f^{-1/2} \quad \text{for } \alpha = 1.5 .$$

The emission measure scales as

$$\text{EM} \propto yF_{obs}U_{in}^{-1}$$

The emission measure is directly related to the intensity of the recombination lines of O and Fe, although variations in temperature, ionization state, and abundances are also important.

4. DISCUSSION

The models described in Table 3 were chosen to have a range of parameters to explore a variety of successful descriptions. Models 1 and 3 both have about the maximum amount of scattering in the hot component relative to the warm component, but have different radial profiles for the gas. Model 2 has a relatively small amount of scattering in the hot component and consequently a different composition (reduced Fe and O abundances). For models 1, 2, and 3 we have assumed

TABLE 4

CALCULATED LINE INTENSITIES

Line	Calculated Flux (10^{-13} ergs cm^{-2} s^{-1})				Observed Flux (10^{-13} ergs cm^{-2} s^{-1})
	Model 1	Model 2	Model 3	Model 4	
O Lyα	4.2	4.4	4.0	4.3	<4.4
Fe L	21	19	22	25	20.0^{+9}_{-6}
Fe Kα	3.9	3.7	4.0	3.9	3.7 ± 2.1
Fe hot	2.7	1.6	4.1	3.9	4.5 ± 2.7

TABLE 5

COLD CLOUD (NLR) MODEL PARAMETERS

Parameter	Value
Composition	High Fe
r_{in} (pc)	450
$n(r_{in})$ (cm^{-3})	7300
$U(r_{in})$	0.0094
τ_{es}	0.0009
f_f	0.009

that the warm component has a covering fraction of about 50%. For all these models it was necessary to extend the hot component to much smaller radii than the warm component in order to produce the observed H-like and He-like Fe recombination lines. In fact, a very small part of the emission from the hot component comes from that part of the hot component sharing volume with the warm component. In other words, the hot component could be terminated at the inner boundary of the warm component without much effect. These models are not natural descriptions of the density profiles, since there is a discontinuity in the total density profile at the inner face of the warm component.

We did attempt to make a model with a more natural total density profile with components in approximate pressure equilibrium. Since the temperatures differ by a factor of about 20, the densities must also. To produce comparable scattering in the warm and hot components, the warm component must have a filling factor or a covering fraction of about 5%. We have assumed a filling factor of 5% and a covering fraction of 1. Scaling from model 3 using the above scaling relations, we find τ_{es} reduced by a factor of 2, r_{in} reduced by a factor of about 10, and n_1 and EM unchanged. Although this model successfully reproduces the observed lines, the scattering region is very small ($<0''.1$), in apparent conflict with the recent *HST* observations.

We have not attempted to produce fully consistent two-phase solutions throughout the overlapping volumes of the warm and hot components. In fact, the ratio of the pressures varies throughout the volumes, and we have not verified that two components can be maintained everywhere in the overlapping regions. Producing a fully consistent model is complex because U changes as a function of radius. This is partly due to the assumed radial density profile for models 1 and 3, but the finite optical depth plays an even more important role. Not only does this cause U to change with radius, but the spectral shape of the ionizing continuum and the relationship between U and T also change with radius. The major cause for this variation is the attenuation of the flux near 1 keV due to the increasing opacity of H-like oxygen ions. We believe the complex modeling required to produce fully consistent two-phase solutions is premature at this time. The models presented should provide a general description of acceptable solutions.

TABLE 6

COLD CLOUD (NLR) MODEL RESULTS

Line	Calculated Flux	Dereddened Flux
Hβ	1.0	1.0
Hα	2.8	2.8
He II λ4686	0.35	0.55
Lyα	29	42
C III] λ1919	8.8	4.0
C IV λ1549	11	9.5
N III] λ1750	0.7	1.0
N IV] λ1486	0.6	1.3
[O II] λ3727	0.3	1.5
[O III] $\lambda\lambda$5007 + 4959	12	17
O III] λ1664	0.4	<0.3
Mg II λ2798	0.9	1.2

NOTE.—Fluxes are relative to dereddened Hβ flux of 3.0×10^{-12} ergs s^{-1}. $E(B-V) = 0.4$ mag, and a simple $1/\lambda$ extinction is assumed.

Although a large number of parameters are used to characterize the models, many are reasonably well constrained. F_{obs} is well determined from the X-ray observations. For the warm component U is constrained by the temperature and lack of absorption, and τ_{es} cannot be much larger than a few percent because of the lack of absorption. The observed equivalent widths of Hβ from different areas of NGC 1068 indicate that y_h must be less than about 50%. We have made what we believe are reasonable estimates for the intrinsic luminosity of NGC 1068 and the solid angle Ω subtended by the scattering region, but we recognize that the values used could be in error. The intrinsic luminosity is based on the observed IR luminosity, but anisotropic IR emission from the torus as suggested by Pier & Krolik (1992) could require changing the assumed luminosity by factor of a few. A large increase in Ω appears incompatible with the *HST* image of the source by Evans et al. (1991). A much smaller opening angle is inconsistent with the simplest form of the unified model of Seyfert galaxies, since the nucleus of only a very small fraction of Seyfert galaxies would be directly visible (and thus called Seyfert 1 galaxies). The effects of changes in these parameters can be estimated using the above scaling relationships. For example, increasing Ω while leaving the intrinsic luminosity constant requires a corresponding decrease in τ_{es}, and leads to $r_{in} \propto \Omega$, $n_1 \propto \Omega^{\alpha-2}$, and no change in the EM. Similarly, increasing the intrinsic luminosity while leaving Ω constant requires a corresponding decrease in τ_{es}, and leads to $r_{in} \propto L^2$, $n_1 \propto L^{2\alpha-3}$, and no change in the EM. We conclude that the densities and positions of the components should be considered rough estimates.

Although only rough estimates can be made of the gas density and location, it is important to recognize that the reduced oxygen abundance is a constant feature of all our models. The abundance of oxygen can be increased by increasing the contribution of the hot component to the X-ray continuum, but the contribution is limited by the MGM observations of $W_{H\beta}$. The "high-Fe" composition models (models 1, 2, and 4) have adopted about the maximum acceptable hot component contribution, and the resulting oxygen abundance is about 5 times less than solar (3 times less if half the soft X-ray flux is due to an extended component). We have shown that the predictions of a simple model for the NLR with such a low abundance are consistent with the observed optical and UV emission.

In general, the determination of the abundance in the nucleus of AGNs is difficult. There is a paucity of adequate X-ray data, but optical data are available for many sources. For example, Bergmann & Pastoriza (1989) found an overabundance of nitrogen relative to oxygen in their survey of six Seyfert 2 and LINER nuclei and interpreted the data in terms of an overabundance of nitrogen rather than an underabundance of oxygen. Winge et al. (1992) report a nitrogen abundance twice solar and oxygen abundance one-third solar for the NLR of the Seyfert 1 galaxy NGC 3783. Most of these determinations are based on the analysis of optical lines. These are quite model-dependent, mainly because of uncertainties in the shape of the ionizing continuum. The case of NGC 1068 is

different, since it is based on the line O III] λ1664 and its strength relative to N III] λ1750, C III] λ1909, and C IV λ1549. In a photoionized gas it is almost impossible to change these ratios without changing the composition. An underabundance of oxygen is somewhat difficult to explain, since the usual stellar evolution mechanisms tend to couple the carbon and oxygen abundances, and nitrogen is partly synthesized from carbon and oxygen. It is not our intention to discuss this problem at length, only to point out the strong evidence for the depletion of oxygen.

Additional components may also contribute to the X-ray spectrum, but we believe such contributions are small. A reflection component from a directly visible segment of the obscuring torus of NGC 1068 is a plausible contributor, but there is no evidence for such a component. A small contribution would cause a small overestimate of the Fe abundance in the warm component (and thus by assumption in the hot component as well). The recent *ROSAT* HRI observation of NGC 1068 (Wilson et al. 1992) indicates that perhaps 45% of the soft X-rays may be from spatially extended components. As a result, the ionizing continuum seen by the scattering medium in the core of NGC 1068 would see a different spectrum than that seen with BBXRT. We have calculated models with such a modified continuum and find that they require a somewhat higher ionization parameter and also have less restrictive upper limits on the abundance of oxygen. However, no successful model could be found without a strong depletion of oxygen, by a factor of at least 2.5. There is little effect on the estimated Fe abundance. The extended components could contribute to the Fe L lines, but the intensity of these lines has not played an important role in our analysis.

5. SUMMARY

The BBXRT observation of NGC 1068 has provided the first moderate-resolution X-ray spectrum of any Seyfert 2 galaxy. The observed X-ray continuum is similar to that observed from other active galaxies, and supports the model in which the observed X-rays are seen through Compton scattering of the X-ray continuum from the nucleus of a Seyfert 1 galaxy at the center of NGC 1068. The multiplicity of the observed Fe K lines requires the existence of a "hot" component of the scattering medium in addition to the "warm" scattering cloud required by the polarized optical light. The relative strengths of the Fe K lines indicate that the two components scatter comparable (within a factor of a few) amounts of radiation.

The warm component produces the Fe Kα line at ~6.4 keV and the Fe L shell emission. The equivalent width of the Fe Kα line indicates that the Fe abundance is at least 65% that of solar and could be several times larger than solar. If most of the scattering occurs in the warm component, $X_{\rm Fe}$ is 1.5 ± 0.85; if there is equal scattering by the warm and hot components, the abundance increases by a factor of 2. The lack of intrinsic absorption and the upper limit on O Lyα emission requires that the abundance of O in the warm component is at least 5 times less than solar. If C and N have solar abundances and the composition of the warm component and the NLR are the same, the line O III] λ1664 from the NLR will be weak compared with N III] λ1749, C III] λ1909, and C IV λ1549. Recent UV observations (Kriss et al. 1992) support this picture.

Based on the relative intensities of the H-like and He-like recombination lines of Fe, the hot component has a sizable fraction of its Fe fully ionized, and its temperature is probably comparable to the Compton temperature ($\sim 4 \times 10^6$) of the radiation from the nucleus. While the hot and warm components may share the same volume in approximate pressure equilibrium, this is not required. In our preferred models, the warm component extended from 20 pc to about 100 pc, while the hot component began at 1 or 2 pc, but these should be viewed as rough indications of the location of the scattering medium.

It is a pleasure to acknowledge our many colleagues at GSFC whose ingenuity and determination were responsible for the development of the BBXRT instrument. We are also grateful to the numerous people who contributed to the success of the *Astro-1* mission. We thank G. Kriss for providing his results prior to publication. H. N. acknowledges a senior NRC research fellowship and BSF grant 89-00179. He also thanks the personnel of the Laboratory for High Energy Astrophysics for their hospitality and help during his sabbatical stay at Goddard.

REFERENCES

Anders, E., & Grevesse, N. 1989, Geochim. Cosmochim. Acta, 53, 197
Antonucci, R. R. J., & Miller, J. S. 1985, ApJ, 297, 621
Arnaud, M., & Raymond, J. 1992, ApJ, 398, 394
Band, D. L., Klein, R. I., Castor, J. I., & Nash, J. K. 1990, ApJ, 362, 90
Bergmann, T. S., & Pastoriza, M. G. 1989, ApJ, 347, 195
Bruhweiler, F. C., Truong, K. Q., & Altner, B. 1991, ApJ, 379, 596
Caganoff, S., et al. 1991, ApJ, 377, L9
Code, A. D., et al. 1991, BAAS, 23, 922
Elvis, M., & Lawrence, A. 1988, ApJ, 331, 161
Evans, I. N., Ford, H. C., Kinney, A. L., Antonucci, R. R. J., Armus, L., & Caganoff, S. 1991, ApJ, 369, L27
Ferland, G., & Osterbrock, D. B. 1986, ApJ, 300, 658
Halpern, J. 1992, Testing the AGN Paradigm, ed. S. S. Holt, S. G. Neff, & C. M. Urry (New York: AIP), 524
Holt, S. S. 1983, in Supernova Remnants and Their X-Ray Emission, ed. J. Danziger & P. Gorenstein (Dordrecht: Reidel), 17
Kallman, T. R., & Mushotzky, R. 1985, ApJ, 292, 49
Kinney, A. L., Antonucci, R. R. J., Ward, M. J., Wilson, A. S., & Whittle, M. 1991, ApJ, 377, 100
Koski, A. T. 1978, ApJ, 223, 56
Koyama, K., et al. 1989, PASJ, 41, 731
Kriss, G. A., Canizares, C. R., & Ricker, G. R. 1980, ApJ, 242, 492
Kriss, G. A., Davidsen, A. F., Blair, W. P., Ferguson, H. C., & Long, K. S. 1992, ApJ, 394, L37
Krolik, J. H., & Kallman, T. R. 1987, ApJ, 320, L5
Krolik, J. H., McKee, C. F., & Tarter, C. B. 1981, ApJ, 249, 422
Laor, A. 1990, MNRAS, 246, 369
Laor, A., & Netzer, H. 1989, MNRAS, 238, 897
Lightman, A. P., & White, T. R. 1988, ApJ, 335, 57
Lockman, F. J. 1991, private communication
Lynds, R., et al. 1991, ApJ, 369, L31
Mathews, W. G., & Ferland, G. J. 1987, ApJ, 323, 456
Miller, J. S., & Goodrich, R. W. 1990, ApJ, 355, 456
Miller, J. S., Goodrich, R. W., & Mathews, W. G. 1991, ApJ, 378, 47 (MGM)
Monier, R., & Halpern, J. P. 1987, ApJ, 315, L17
Netzer, H. 1990, in Active Galactic Nuclei (Berlin: Springer-Verlag), 57
Neugebauer, G., et al. 1980, ApJ, 238, 502
Pier, E. A., & Krolik, J. H. 1992, BAAS, 23, 1469
Pogge, R. W. 1988, ApJ, 328, 519
Pounds, K. A., Nandra, K., Stewart, G. C., George, I. M., & Fabian, A. C. 1990, Nature, 344, 132
Rees, M. J., Netzer, H., & Ferland, G. J. 1989, ApJ, 347, 640
Serlemitsos, P. J., et al. 1992, in Proc. 28th Yamada Conf., Frontiers of X-Ray Astronomy (Tokyo: Universal Academy)
Shields, G. A., & Oke, J. B. 1975, ApJ, 197, 5
Snijders, M. A. J., Netzer, H., & Boksenberg, A. 1986, MNRAS, 222, 549
Telesco, C. M., Becklin, E. E., Wynn-Williams, C. G., & Harper, D. A. 1984, ApJ, 282, 427
Weaver, K. A. 1993, Ph.D. thesis, Univ. Maryland, in preparation
Wilson, A. S., Elvis, M., Lawrence, A., & Bland-Hawthorn, J. 1992, ApJ, 391, L75
Winge, C., Pastoriza, M. G., Storchi-Bergmann, T., & Lipari, S. 1992, ApJ, 393, 98